KSME

Springer

Journal of Mechanical Science and Technology 38 (5) 2024

Original Article
DOI 10.1007/s12206-024-0417-1

Keywords:
· Laser welding
· Hatching patch
· Circular path
· Aluminum
· Stainless steel
· Lithium-ion battery

Correspondence to:
Dongkyoung Lee
ldkkinka@kongju.ac.kr

Citation:
Trinh, L., Lee, D. (2024). Effect of welding path on the weld quality of aluminum tab and steel battery case in lithium-ion battery. Journal of Mechanical Science and Technology 38 (5) (2024) 2385~2395. http://doi.org/10.1007/s12206-024-0417-1

Received March 29th, 2023
Revised January 5th, 2024
Accepted January 21st, 2024

† Recommended by Editor Chongdu Cho

Effect of welding path on the weld quality of aluminum tab and steel battery case in lithium-ion battery

Lanh Trinh[1,2] and Dongkyoung Lee[2,3,4,5]

[1]Department of Mechanical and Materials Engineering, University of Nebraska–Lincoln, Lincoln 68588, NE, USA, [2]Department of Future Convergence Engineering, Kongju National University, Cheonan 31080, Korea, [3]Department of Mechanical and Automotive Engineering, Kongju National University, Cheonan 31080, Korea, [4]Center for Advanced Powder Material and Parts (CAMP[2]), Kongju National University, Cheonan 31080, Korea, [5]Global Institute of Manufacturing Technology (GITECH), Kongju National University, Cheonan 31080, Korea

Abstract The choice of welding path in joining battery connections plays a crucial role in the bonding strength, which in turn affects battery performance. A commonly employed welding path in laser welding is the circular wobbling path. Our prior study revealed that the hatching path in laser welding, which is hardly reported in the literature, offers a flexible welding pattern and sufficient weld strength, especially for thin specimens. This study conducted a comparative analysis of circular and hatch welding paths concerning their microstructure, mechanical properties, and electrical characteristics. Upon observing the surfaces of the two types of welds, it becomes evident that the hatch welding path results in a superior weld appearance with less spatter formation near the welding zone in comparison to the circular path. Furthermore, an examination of the cross-sections reveals a significant disparity in the interdiffusion between the welding materials. While the circular path yields a non-uniform chemical diffusion of the case material within the welded tab, the hatching path exhibits a periodic upward penetration of the case material into the tab at the welding lines. This discrepancy leads to a distinctive distribution of hardness, electrical resistance, and mechanical strength in the welds, with the desired properties attributed to the hatch welding path. Through this comparative analysis, the study unveils the influence of the laser beam deflection path on the overall weld quality.

1. Introduction

Lithium-ion batteries (LIBs) have become a crucial part of electronic devices, electric vehicles, as well as energy storage systems for a long history [1-3]. Their widespread adoption is attributed to their extended lifespan, high energy density, robust power density, and positive environmental impact [4]. However, the demand for more powerful and higher-capacity batteries continues to grow as global consumer expectations rise. In response, continuous enhancements are being made in different aspects of battery design, encompassing material selection and manufacturing processes, aiming to not only reduce production costs but also improve battery efficiency [5]. Historically, materials like $LiCoO_2$ for cathodes and graphite for anodes were chosen for battery electrodes. These selections have persevered over time [6-8]. However, present-day research focuses on refining LIB manufacturing procedures with alternative technologies, with significant attention on the joining process, as it significantly influences battery capacity [9-17]. In LIBs, joints can be categorized into electrical and structural types, and many joints, such as those connecting tabs and battery cases, must meet both electrical and structural requirements. These connections often involve materials of varying thicknesses and dissimilar compositions, sometimes even in challenging positions. Commonly, aluminum (Al) is used for the tab, while steel (Fe-based alloy) is used for the battery case. The interdiffusion of these metals, stemming from the low solubility of Al and Fe, results in the formation of intermet

allic compounds (IMCs). IMCs typically possess complex crystal structures with limited crystallographic planes, making them prone to stress-related issues. IMCs are generally brittle, negatively impacting joint quality by causing crack initiation and impeding current flow through the materials [9, 18-20]. Thus, minimizing the presence of IMCs is essential for achieving high-quality welds.

Various joining technologies have been employed in LIBs production, including resistance spot welding and ultrasonic welding. Researchers and manufacturers have extensively explored resistance spot welding for dissimilar Al and Fe metals, investigating factors affecting joint properties and proposing techniques to control interfacial reactions [21]. Although research on resistance spot welding for Al and steel was conducted widely in the past [22-25], this approach faces challenges, such as electrode degradation, damaged weld surfaces, and material limitations [24-26]. On the other hand, ultrasonic welding, another widely used technique for joining Al and steel in industries like automotive, shipbuilding, and electronics, offers a sound joint for such dissimilar metals [27-30]. However, as a contact process, ultrasonic spot welding is notably influenced by tool properties, with tool wear being a concern. To overcome these challenges, a remote and flexible welding technology is needed.

Since its inception, the laser beam has found applications in various manufacturing stages, including heat treatment, annealing, cutting, drilling, and welding [31-34]. Laser beam welding stands out for its contactless nature, offering flexible weld configurations with high precision. Its high focus results in a small heat-affected zone, making it ideal for heat-sensitive components. Research indicates that laser beam welding often outperforms traditional joining methods [35]. Moreover, the development of IMCs in dissimilar metal joints is closely tied to the interdiffusion of these metals. Laser welding, with its high cooling rate, accelerates the rapid solidification process, consequently minimizing the aging duration of the diffused dissimilar metals. This, in turn, leads to a reduction in the formation of IMCs.

The non-contact nature of laser welding allows a flexible design of welding geometry. Wobbling welding, where the laser beam oscillates the focal spot in a circular shape, is commonly employed due to bonding effectiveness [36]. Moreover, Kuryntsev et al. [37] found that the wobbling technique significantly improved the mechanical properties, as well as minimized phased transitions due to a lower cooling rate. Moreover, the weld strength is enhanced by enlarging the bonding area with wobbling welding [36]. In addition, Wang et al. [38] pointed out the effect of the circular oscillation technique on the weld quality by decreasing the thermal gradient. As a result, the formation of equiaxed grain is promoted, while columnar dendrites are minimized. To offer more flexibility in terms of beam movement, the hatching path was introduced, mainly applied in additive manufacturing [39-41]. Our previous study revealed the possibility of laser welding with a hatching path [9, 42], especially for a thin specimen. Both wobbling and hatching techniques have the advantage of increasing the bonding area with the same bead width. To further evaluate the effectiveness of the hatching path compared to the conventional wobbling path, microstructure, mechanical properties and electrical conductivity of the welds created from these paths need to be investigated. However, a comprehensive comparison of these two welding paths concerning weld quality is lacking.

This study conducted a comprehensive comparison of two welding paths, hatching and circular, in terms of the morphology, mechanical properties, and electrical properties of dissimilar metal joints involving Al and steel. For this comparison, constant total energy input and laser parameters were maintained in both welding paths, with identical lengths for the laser irradiation path. Scanning electron microscopy (SEM) was employed to examine the weld surface and observe spatter formation. Energy dispersive X-ray spectroscopy (EDX) was used to analyze chemical diffusion in the weld. The study also includes measurements of hardness distribution, mechanical strength, and electrical conductivity to assess the performance of the welds.

2. Experiment

2.1 Experimental procedure

The welding experiment was conducted with a pulsed fiber laser, the specification of the laser source is indicated in Table 1. The laser source used in the experiment is an ytterbium pulsed fiber laser (IPG-YLPM, IPG photonics, Southbridge, Massachusetts USA). The laser beam is transferred through a focusing lens, which has a working distance of 189 mm. The weld is performed in a lap welding configuration, with pure aluminum (purity 99 %) on the top of commercial 304 stainless steel having a thickness of 0.087 mm and 0.4 mm, respectively. The optimization for selected laser parameters can be found in our prior study [42]. The aluminum and stainless steel represent the material selection for the battery case and tabs, respectively.

The weld is conducted in two different welding paths, namely hatching and circular oscillation paths shown in Fig. 1. In the hatching path, the laser beam first irradiates in a rectangular shape ①. As the rectangular irradiation closes, hatching welding is performed inside the rectangle ②. The hatching lines are created in zigzag lines with the distance between the two lines

Table 1. Specifications and parameters of the laser welding source.

Ytterbium pulsed fiber laser	
Laser power	10-20 W
Wavelength	1064 nm
Pulse duration	200 ns
Spot size	30 μm
Repetition rate	20 kHz
Welding speed	1 mm/s

being 0.1 mm. Whereas, the circular path is performed by oscillating the laser irradiation in a circular path with a diameter of 0.5 mm. The selected amplitude and frequency for the circular welding path are to be comparable processing time given by the total welding length (L) and welding one dimension to the hatching path. The dimensions of the welding zone are 0.5 mm wide and 4.5 mm long. The total length of the welding line is calculated as follows:

Hatching path: The hatching path (Fig. 1(b)) is created by a rectangular boundary and hatching lines inside it. Therefore, the total length of the hatching path is:

Total length (L) = Circumference of the rectangular + total length of hatching lines = 28.5 (mm)

Circular path: One cycle in a circular welding path (Fig. 1(c)) is composed of half of the cycle (top part) and half of the ellipse (bottom part). Therefore, the total length of the circular path is:

Total length (L) = (½ circular circumference + ½ elliptical circumference) × 20 = 28.44 (mm)

The surface morphology and microstructure of the weld cross-section were observed using a scanning electron microscope (SEM) equipped with an energy-dispersive X-ray spectroscopy (EDX) detector (Mira CMH, TESCAN, Brno, Czech Republic). Prior to characterization, the joint is embedded in a resin medium for handling during polishing. The sample is ground using sandpaper with grid sizes ranging from 600 to 1200. Subsequently, a 0.5 μm diamond suspension is employed to polish the sample, resulting in a mirror-like finished surface. Vickers microhardness measurements of the weld were conducted with a Mitutoyo HM-100 series microhardness machine, applying a load of 0.49 N for a dwell time of 10 seconds. Joint strength testing was carried out using a universal testing machine (Shimadzu Ag-X Plus, Shimadzu Europa GmbH, Duisburg, Germany) with a loading speed of 0.5 mm/min. To measure electrical resistance across the joint, a four-point resistance measurement system was employed, utilizing a high-precision voltmeter from the Keithley Integra Series Model 2460 ohmmeter.

3. Results and discussion

3.1 Weld surface observation

Fig. 2 presents an observation of the top surface of the weld with the hatching path and the circular path. Notably, in both

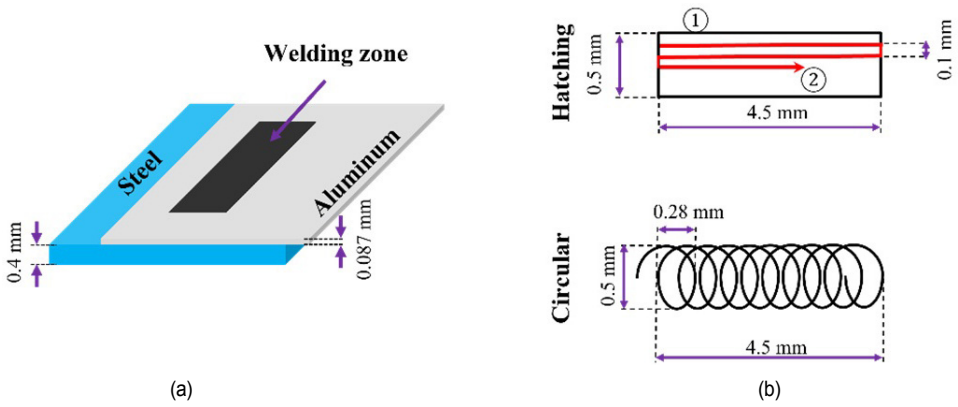

Fig. 1. Welding path: (a) hatching path; (b) circular path.

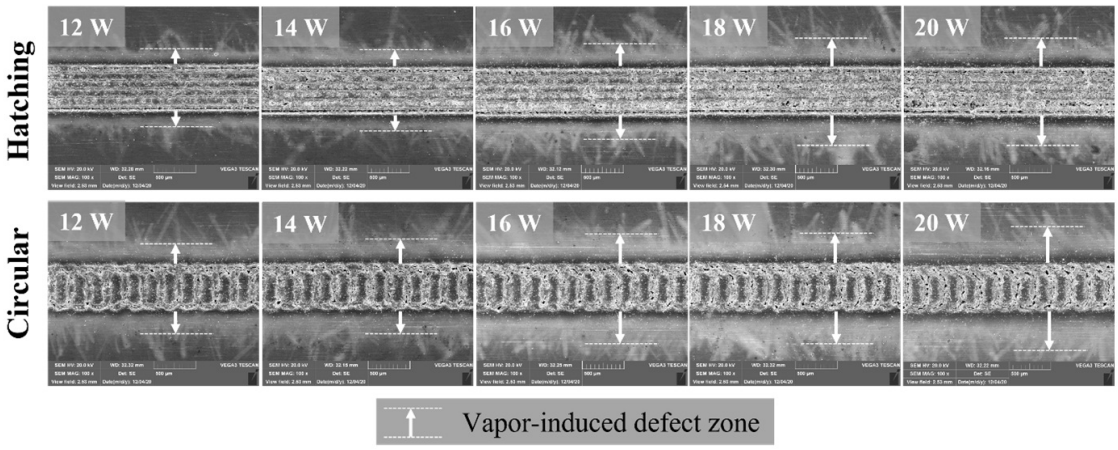

Fig. 2. Top view of the weld.

welding paths, there is a vapor-induced defect zone, which arises from the metal vapor generated during the evaporation of molten materials while welding. Fig. 3 demonstrates that the circular path welding results in a slightly larger vapor-induced defect compared to the hatching path. Additionally, at the intersection of each pair of cycles, as explained in Ref. [42], explosive holes are formed. These explosive holes are visible in the top view of the weld shown in Fig. 3 and they tend to expand as laser power increases. Furthermore, there is the formation of spatters on the weld surface. It is essential to minimize spatter formation in electrical application joints, as spatters can introduce changes in the microstructure of the materials where they land, thereby impacting the electrical properties of the joint. Given the current limitations in quantifying spatter formation within the weld zone, measurements of spatter distribution, specifically the spatter area, were conducted for comparison. The spatter area is acquired through the software ImageJ with the measurement principle described in Ref. [43]. Before image processing, SEM images of spatter formation were taken at a distance of 100 μm from the boundary of the welding line at both the top and bottom of the welding area. For quantifying spatters, three different regions of interest, each with a size of 200 μm × 200 μm, were employed. The results for the spatter area measurement on the weld surface at both the top and bottom areas are shown in Fig. 4.

The data clearly indicate that the spatter formed on the top area is larger than that on the bottom area. This discrepancy can be attributed to the characteristics of each welding path. In the hatching path, welding commences at the bottom area and concludes at the top area. During the welding process, the top area is heated, which reduces the surface tension of the materials in that region, leading to increased spatter formation. Conversely, in the circular path, more intersections of the welding path occur in the top area compared to the bottom area. At each intersection, spatter is contributed by both the initial welding path and the subsequent welding path intersecting with it.

Fig. 4 highlights the disparity in spatter formation between the hatching and circular welding paths. Generally, the circular path exhibits a larger spatter area on the weld surface compared to the hatching path. Furthermore, as laser power increases, the spatter area expands. This result can be reliably explained by the specific design of the welding paths. Spatters tend to eject in the opposite direction of the laser irradiation movement [44]. The circular welding path follows a circular movement, while the hatching path is characterized by parallel lines. As a consequence, from the boundary line of the welding zone, different welding directions are observable in the case of the circular path. In contrast, the hatching path maintains a consistent parallel direction with the boundary line. Thus, owing to the circular movement and the increased number of intersections between cycles, the circular path generates a larger spatter area in comparison to the hatching path.

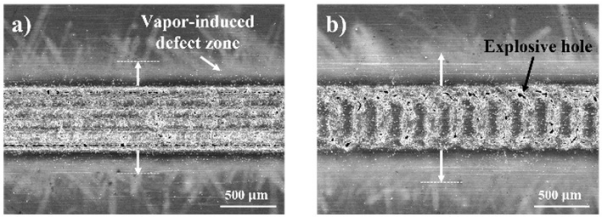

Fig. 3. Top view observation at the laser power of 16 W: (a) hatching path; (b) circular welding path.

3.2 Cross-section observation

Figs. 5 and 6 depict SEM images of the cross-sections of welds conducted at laser powers of 14 W and 16 W, respectively. In both welds, there is a noticeable upward penetration (UP) of stainless steel into the aluminum, a phenomenon previously reported in a prior study [42, 45], This UP effect is believed to enhance the overall strength of the joint, especially in the context of overlap welding with aluminum positioned atop stainless steel. While the hatching path results in periodic UP occurrences at each hatching line, the circular welding path exhibits two prominent UP regions on the sides of the pattern. However, this UP effect leads to an insufficient presence of molten material at the bottom layer, resulting in the formation of

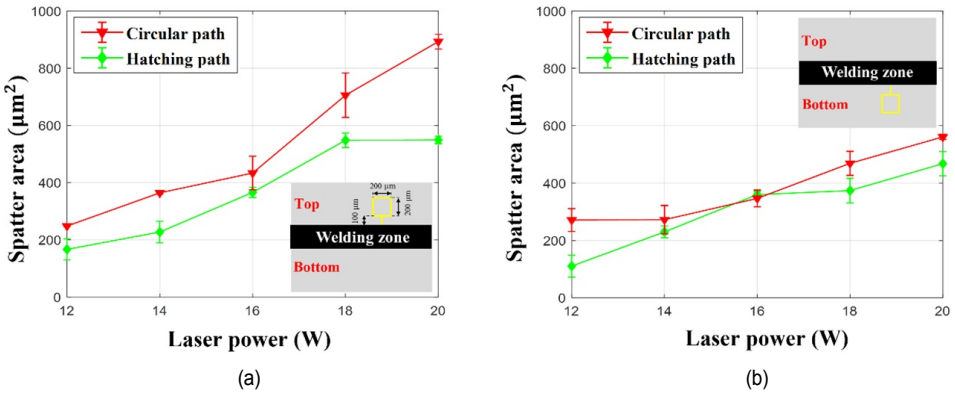

Fig. 4. Spatter area on the weld surface: (a) top; (b) bottom.

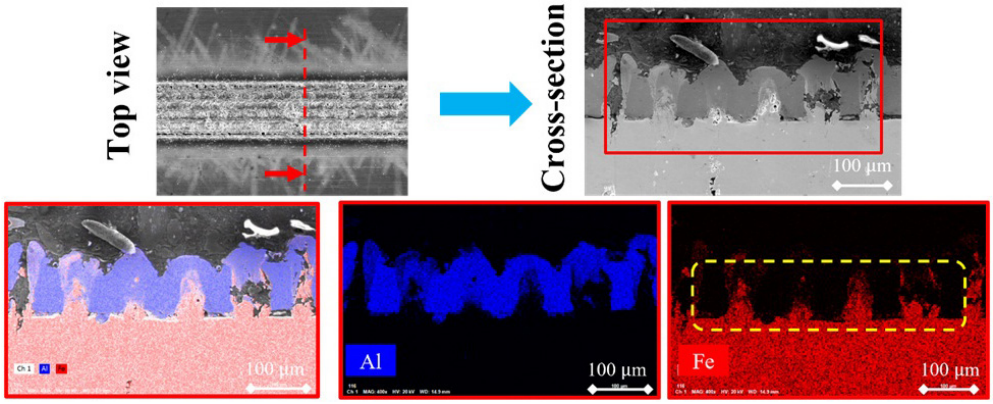

(a)

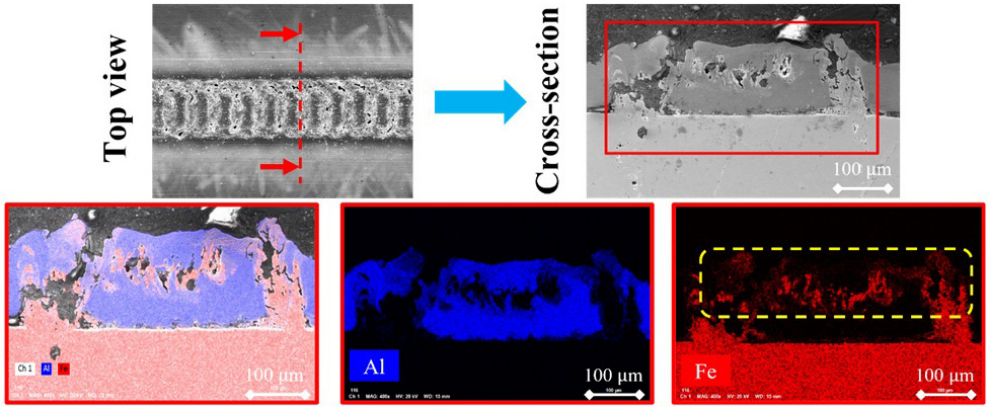

(b)

Fig. 5. EDX mapping result on the cross-section of the welds: (a) hatching path; (b) circular path (14 W).

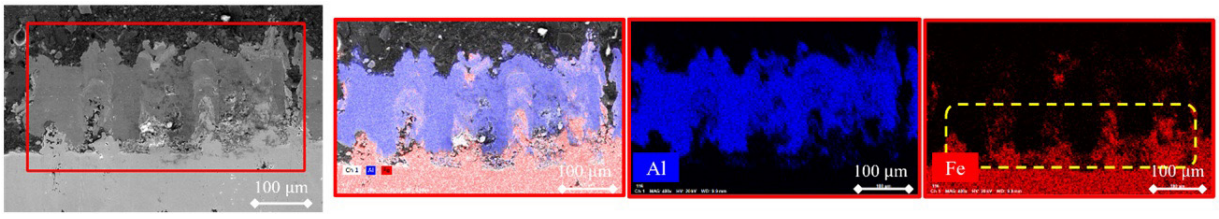

(a)

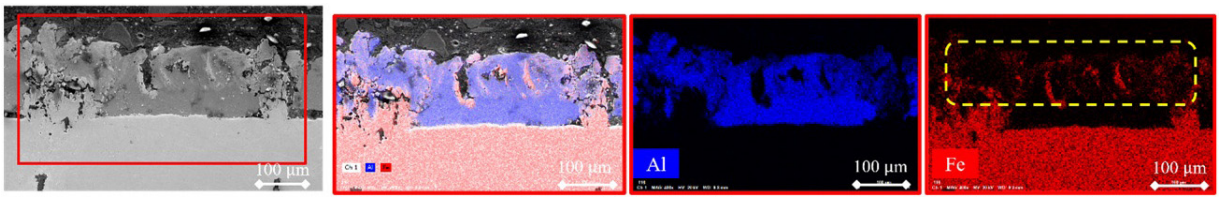

(b)

Fig. 6. EDX mapping result on the cross-section of the welds (16 W): (a) hatching path; (b) circular path.

porosities in this area. Both welds display various defects, including pores, cracks, and explosive holes. Notably, the circular welding path experiences more severe damage from defects, which can be attributed to repeated laser irradiation at the intersections of the weld lines. Furthermore, a breakdown of the upper aluminum material occurs as a consequence of excessive laser irradiation at these intersections, as observed in the cross-section of the circular welding path.

Energy dispersive X-ray (EDX) mapping is employed to observe the diffusion of the welded materials in the welding zone. Figs. 5 and 6 (added to compare the result at different laser powers) exhibit the distribution of the diffused materials in the

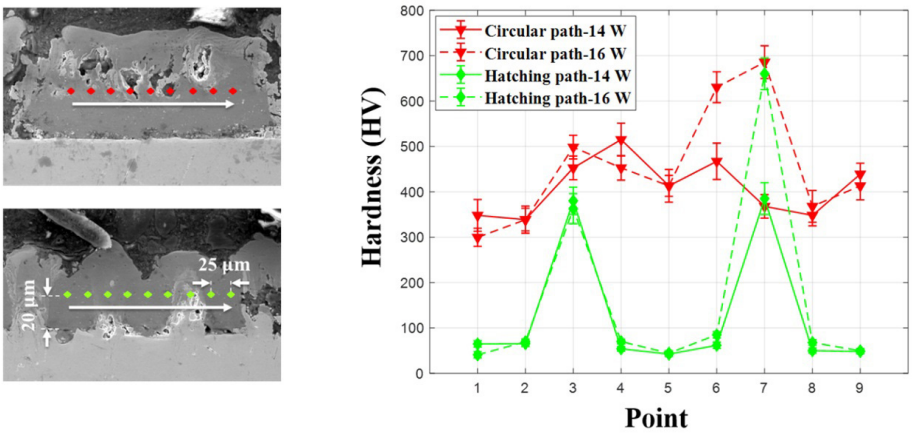

(a) (b)

Fig. 7. (a) Hardness measurement on the cross-section; (b) hardness distribution of weld with hatching and circular paths.

weld with hatching and circular paths at the laser power of 14 W and 16 W, respectively. In general, material diffusion involves the lower material (Fe) diffusing into the upper material (Al). In the hatching path weld, diffused Fe is primarily concentrated at the lower part of the upper material. Additionally, when comparing the laser powers of 14 W and 16 W, it is evident that the diffusion and penetration of Fe into Al increase as laser power increases in the hatching path. In contrast, in the circular welding path, the diffusion of the lower material into the upper material is unevenly distributed, primarily at the top part of the upper material. In the hatching path, the uniform diffusion of Fe into Al suggests that potential intermetallic compounds (IMCs) may only form at the interface of these materials. Conversely, the random distribution of Fe within Al in the circular path can lead to the formation of more IMCs, resulting in brittle material and reduced mechanical properties of the weld metal. The formation of IMCs in the fusion joining techniques arises from the solubility of base materials, leading to the precipitation of ordered structures. For instance, in dissimilar joints between Fe-based alloys and Sn-Pb alloys, IMCs manifest as a continuous layer at the interface, driven by metallurgical reactions between the materials [46]. Additionally, a thick diffusion-influenced layer, induced by high heat, results in the formation of various intermediate phases at the interface of dissimilar metal joints [47].

In the context of this study, the Al layer is anticipated to be fully melted, while the substrate undergoes partial melting, facilitating the easy diffusion of Fe into the Al liquid phase. Within the hatching geometry, a melt pool is generated along each hatching line, leading to periodic upward penetration and subsequent diffusion of Fe into Al. Conversely, a more intricate configuration arises in wobbling welding, where the oscillation of the laser beam causes a melt pool to form across the welding area. Consequently, a broad diffusion area of Fe into Al emerges, promoting the development of a complex intermediate phase (i.e., IMCs) and microstructure [48]. The EDS mapping result in Fig. 6 illustrates a significant difference in chemical composition distribution on the cross-section of the weld in hatching and wobbling modes, aligning with the explanation above.

3.3 Hardness profile

Vickers hardness is conducted in a horizontal direction at a distance of 20 μm from the interface of the upper and lower materials. Fig. 7 presents the hardness profile of the weld with hatching and circular paths. Broadly, it is evident that the circular path exhibits high hardness along the measurement line, whereas the hatching path welding achieves high hardness primarily at the hatching lines. Specifically, in the weld with the circular path at a laser power of 14 W, the hardness remains consistently above 300 HV, albeit with some fluctuations during measurement. Conversely, the weld produced with the hatching path displays notably high hardness, approximately 400 HV, at the positions of the hatching lines. Similarly, at a laser power of 16 W, the hardness distribution along the measurement line in the circular path consistently exceeds 300 HV, while the high hardness profile of the hatching path weld shows hardness values of 362.8 HV and 660.2 HV at the hatching line positions.

The major factors influencing the hardness in the welds include refined microstructure induced by laser welding and IMCs formation. On the one hand, short laser-materials interaction time in pulsed laser welding provides a rapid cooling of molten materials. As reported in the literature, the cooling rate in laser melting can reach up to 105-106 K/s, depending on processing parameters [49]. Such a high cooling rate results in a large undercooling (ΔT), also known as supercooling. The larger the undercooling is, the finer the microstructure including grain size can form. Grain and phase boundaries can effectively act as barriers to dislocation motion, strengthening the materials. Therefore, a fine microstructure provides a high density of the boundaries, improving the strengthening effect. On the other hand, the relatively high hardness distribution within the upper material of the weld with the circular path is due to the random

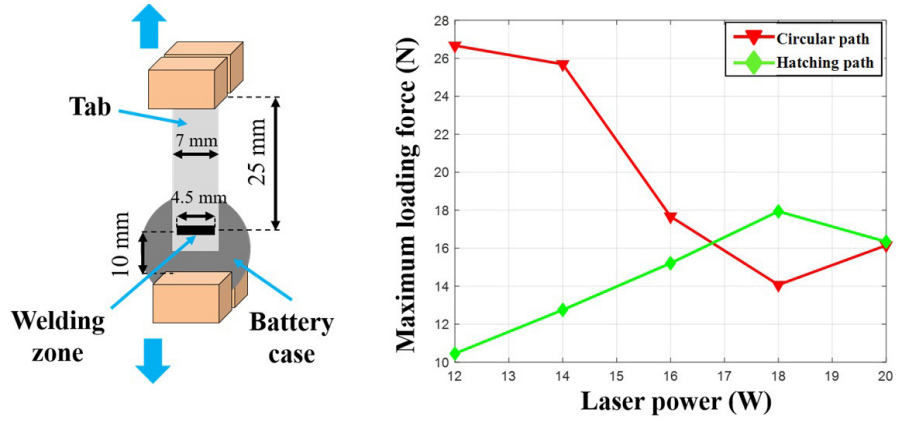

(a) (b)

Fig. 8. Mechanical strength of the weld: (a) measurement setup; (b) mechanical strength.

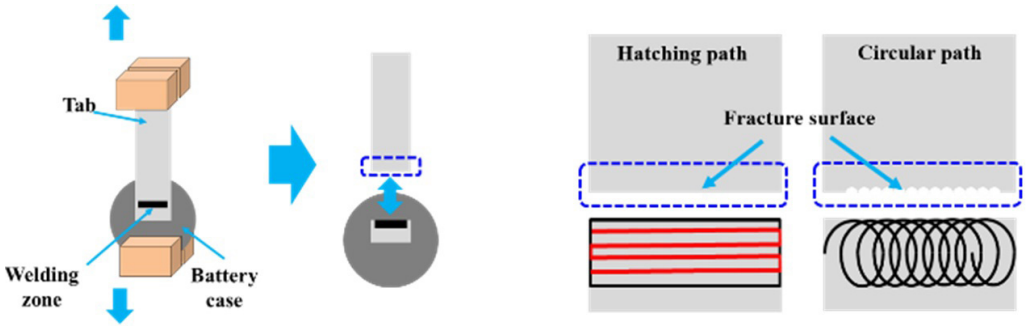

(a) (b)

Fig. 9. Fracture mechanism: (a) strength test; (b) fracture surface.

diffusion of the Fe into the Al, which is evidence for the existence of the IMCs. Conversely, in the hatching path weld, the penetration of the lower material into the upper material occurs primarily at the hatching line positions, accounting for the peak hardness observed at those locations. Generally, the high hardness profile of the circular path weld may result in the formation of porosities and the initiation of cracks, which are considered significant detriments to weld quality.

3.4 Mechanical properties

The mechanical strength of the weld is evaluated by a shear strength test. Fig. 8(a) demonstrates the shear strength test for the welds. The result of the strength test of the weld with hatching and circular paths is shown in Fig. 8(b). Overall, the joint with hatching and circular paths exhibits an opposite tendency. As the laser power increases, the weld with a hatching path results in increasing weld strengths, while the strength of the weld with a circular path tends to decrease. Particularly, at a laser power of 12 W, the strength of the weld with the hatching path reaches the maximum loading force of 10.45 N. As the laser power increases, the loading force that the weld can restrain increases and reaches a peak of 17.94 N at the laser power of 18 W. In comparison, the weld with a circular path suffers from a loading force of up to 26.67 N at laser power of 12 W. However, with the increase of laser power, the force decreases linearly and touches the bottommost with a loading force of 14.07 N at the laser power of 18 W.

The difference in the tendency of the weld strength of the hatching and circular paths can be explained based on the fracture mechanism of the weld. As illustrated in Fig. 9, the fracture of the weld in both welding paths happens at the top boundary of the welding zone. Meanwhile, the fracture surface of the weld with different welding paths is also different. The hatching path produces a relatively flat fracture surface, while the circular path tends to have a wavy fracture surface, as shown in Fig. 10. The flat surface will allow the crack to propagate easily, while crack propagation is difficult on the wavy fracture surface. Thus, the wavy fracture surface makes it harder to fracture in comparison with the flat fracture surface in the hatching path. However, the existence of the explosive hole at the top part of the welding zone in a circular welding path is the main cause of the fracture. As analyzed above, the explosive hole extends as the laser power increases. This leads to a decrease in the weld strength in the circular welding path as the laser power increases. Whereas the weld with the hatching path is strengthened with the increasing laser power due to the increase in penetration depth.

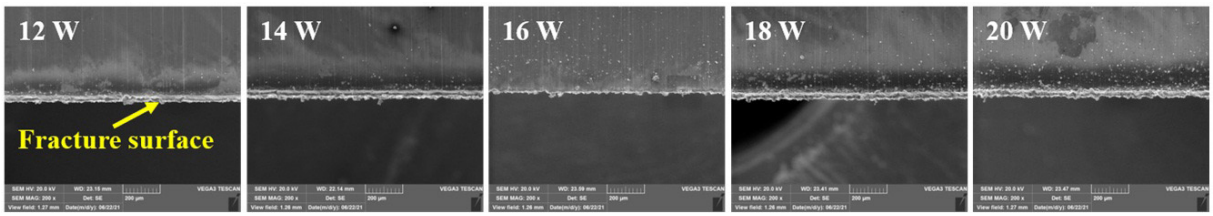

(a)

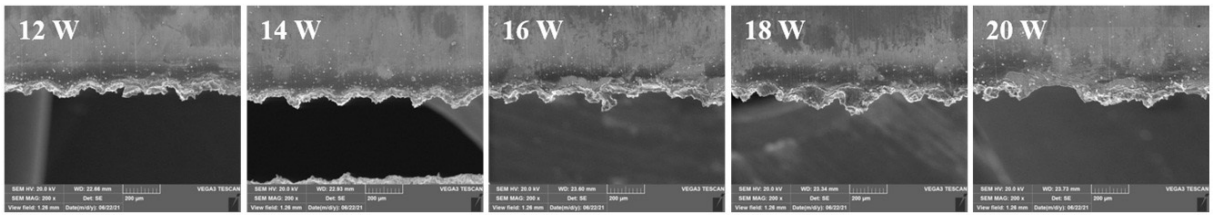

(b)

Fig. 10. Fracture surface observation: (a) hatching path; (b) circular path.

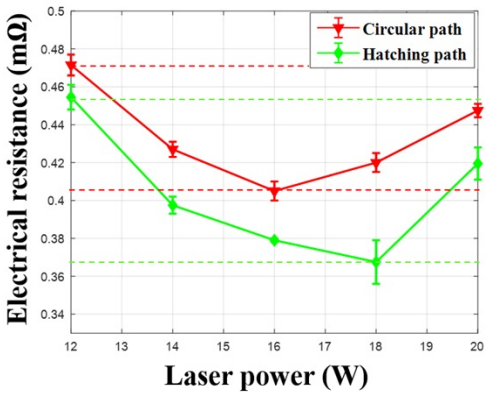

Fig. 11. Electrical resistance of the weld with hatching and circular paths.

3.5 Electrical conductivity

A four-wire measurement method, which is a common resistance measurement method for low electrical resistance [50], was employed to obtain the electrical resistance of the weld with hatching and circular paths. The result of the electrical resistance measurement is shown in Fig. 11. The presented result shows that there is a moderate change in the resistance of the weld using hatching and circular paths when the laser power increases. Meanwhile, the electrical resistance in the hatching and circular paths is within recognizable ranges. The weld with a hatching path reports a lower range of electrical resistance from 0.37 mΩ to 0.45 mΩ in comparison with the circular path which has an electrical resistance from 0.41 mΩ to 0.47 mΩ with the given range of laser power. The higher range of electrical resistance in the weld with a circular path can be explained by the formation of explosive holes and uneven interdiffusion of the upper and lower materials in the weld zone. The fluctuation of the electrical resistance of the weld can be explained by the combined effect of both the formation of IMCs and the penetration of the weld. As analyzed before, the laser power is proportional to the diffusion of the weld materials. Thus, more diffusion of the weld materials possibly results in a higher amount of IMC formation, which increases the electrical resistance. Meanwhile, as the laser power increases, the penetration of the lower material into the upper material also increases. This helps strengthen the weld as well as increases the electrical conductivity of the weld. Thus, the combination of the influence of IMCs and the strength of the weld results in the fluctuation of the electrical resistance in both welds.

4. Conclusion

In addition to the widely adopted circular oscillation technique in laser welding, the potential benefits of a hatching path for enhancing welding bond strength have received comparatively less attention. This study offers a comparative analysis of welds created using two distinct welding paths: the hatching path and the circular path. The quality of these welds is assessed in terms of microstructure, mechanical properties, and electrical properties, leading to several noteworthy conclusions:

1) The circular welding path produces a welding surface with more spatter near the welding zone and is prone to the formation of explosive holes compared to the hatching path. It is advisable to avoid overlapping laser irradiation in the welding path to prevent explosive hole formation.

2) Within the circular welding path, the oscillation of the welding line results in a non-uniform upward penetration (UP) of stainless steel into aluminum, while the hatching path generates periodic UP at each hatching line. Consequently, the circular path yields consistently high hardness varying around 350 HV to 670 HV, whereas the hatching path exhibits periodic peak hardness distribution up to 650 HV within the weld zone.

3) Within the investigated parameter, the strength of welds created with the circular welding path achieves a maximum loading force of 26.8 N and 26 N at 12 W and 14 W, respec-

tively, which is higher than that produced with the hatching path at lower laser power levels. However, this trend reverses as laser power increases where the loading reduces around 15 N, primarily due to the expansion of explosive holes.

4) The circular path results in welds with electrical resistance ranging from 0.41 mΩ to 0.47 mΩ, whereas the hatching path welds exhibit resistances between 0.37 mΩ to 0.45 mΩ as the laser powder increases from 12 W to 20 W.

Circular and hatching paths offer distinct advantages in enhancing joint quality. Nevertheless, this study primarily focuses on comparing these two approaches. To further enhance weld strength using the hatching path, further investigations into strengthening methods are recommended.

Acknowledgments

The research described herein was supported by the National Research Foundation of Korea (NRF) (No. RS-2023-00208039) and by the Innopolis Foundation of Korea (No. 2023-SB-SB-0079) funded by the Ministry of Science and ICT (MSIT, Korea). This research was also supported by the Regional Innovation Strategy (RIS) (2021RIS-004) through the National Research Foundation of Korea (NRF) funded by the Ministry of Education (MOE, Korea). In addition, this work was supported by the Technology Development Program (S3288700, S3275266) funded by the Ministry of SMEs and Startups (MSS, Korea), and by the Korea Institute for Advancement of Technology (KIAT) (P0018009) funded by the Ministry of Trade, Industry, and Energy (MOTIE, Korea). The opinions expressed in this paper are those of the authors and do not necessarily reflect the sponsors' views.

References

[1] S. Megahed and W. Ebner, Lithium-ion battery for electronic applications, *J. Power Sources*, 54 (1) (1995) 155-162, doi: 10.1016/0378-7753(94)02059-C.

[2] N. Nitta, F. Wu, J. T. Lee and G. Yushin, Li-ion battery materials: Present and future, *Mater. Today*, 18 (5) (2015) 252-264, doi: 10.1016/j.mattod.2014.10.040.

[3] T. Chen et al., Applications of lithium-ion batteries in grid-scale energy storage systems, *Trans. Tianjin Univ.*, 26 (3) (2020) 208-217, doi: 10.1007/s12209-020-00236-w.

[4] R. Ravi, *Importance of Lithium Ion Battery in BMS of Electric Vehicles*, ResearchGate (2020) doi: 10.13140/RG.2.2.20898.66241.

[5] A. Yoshino, *Development of the Lithium-Ion Battery and Recent Technological Trends*, Elsevier, Netherlands (2014) doi: 10.1016/B978-0-444-59513-3.00001-7.

[6] T. Fujita and K. Toda, Microdisplacement measurement using a liquid-delay-line oscillator, *Japanese J. Appl. Physics, Part 1 Regul. Pap. Short Notes Rev. Pap.*, 42 (9) (2003) 6131-6134, doi: 10.1143/jjap.42.6131.

[7] J. B. Goodenough and K. Mizushima, *Fast ION Conductors*, United States Patent (1982) https://patents.google.com/patent/US4357215A/en.

[8] R. Yazami and P. Touzain, A reversible graphite-lithium negative electrode for electrochemical generators, *J. Power Sources*, 9 (3) (1983) 365-371, doi: 10.1016/0378-7753(83)87040-2.

[9] L. N. Trinh and D. Lee, The effect of using a metal tube on laser welding of the battery case and the tab for lithium-ion battery, *Materials (Basel)*, 13 (19) (2020) 4460, doi: 10.3390/ma13194460.

[10] D. Lee, R. Patwa, H. Herfurth and J. Mazumder, High speed remote laser cutting of electrodes for lithium-ion batteries: anode, *J. Power Sources*, 240 (2013) 368-380, doi: 10.1016/j.jpowsour.2012.10.096.

[11] D. Lee, B. Oh and J. Suk, The effect of compactness on laser cutting of cathode for lithium-ion batteries using continuous fiber laser, *Appl. Sci.*, 9 (1) (2019) 205, doi: 10.3390/app9010205.

[12] D. Lee, R. Patwa, H. Herfurth and J. Mazumder, Computational and experimental studies of laser cutting of the current collectors for lithium-ion batteries, *J. Power Sources*, 210 (2012) 327-338, doi: 10.1016/j.jpowsour.2012.03.030.

[13] J. Godek, Joining lithium–ion batteries into packs using small-scale resistance spot welding, *Weld. Int.*, 27 (8) (2013) 616-622, doi: 10.1080/09507116.2011.606148.

[14] D. Lee and S. Ahn, Investigation of laser cutting width of Li-CoO_2 coated aluminum for lithium-ion batteries, *Appl. Sci.*, 7 (9) (2017) 914, doi: 10.3390/app7090914.

[15] A. Das, D. Li, D. Williams and D. Greenwood, Weldability and shear strength feasibility study for automotive electric vehicle battery tab interconnects, *J. Brazilian Soc. Mech. Sci. Eng.*, 41 (1) (2019) 1-14, doi: 10.1007/s40430-018-1542-5.

[16] Y. T. You and J. W. Kim, Fiber laser welding properties of copper materials for secondary batteries, *Medziagotyra*, 23 (4) (2017) 398-403, doi: 10.5755/j01.ms.23.4.16316.

[17] M. F. R. Zwicker, M. Moghadam, W. Zhang and C. V. Nielsen, Automotive battery pack manufacturing – A review of battery to tab joining, *J. Adv. Join. Process.*, 1 (2019) (2020) 100017, doi: 10.1016/j.jajp.2020.100017.

[18] Y. Xue, R. Shen, S. Ni, M. Song and D. Xiao, Fabrication, microstructure and mechanical properties of Al-Fe intermetallic particle reinforced Al-based composites, *J. Alloys Compd.*, 618 (2015) 537-544, doi: 10.1016/j.jallcom.2014.09.009.

[19] C. Dharmendra, K. P. Rao, J. Wilden and S. Reich, Study on laser welding-brazing of zinc coated steel to aluminum alloy with a zinc based filler, *Mater. Sci. Eng. A*, 528 (3) (2011) 1497-1503, doi: 10.1016/j.msea.2010.10.050.

[20] A. Mathieu et al., Dissimilar material joining using laser (aluminum to steel using zinc-based filler wire), *Opt. Laser Technol.*, 39 (3) (2007) 652-661, doi: 10.1016/j.optlastec.2005.08.014.

[21] M. Pouranvari, Critical assessment: dissimilar resistance spot welding of aluminium/steel: challenges and opportunities, *Mater. Sci. Technol. (United Kingdom)*, 33 (15) (2017) 1705-1712, doi: 10.1080/02670836.2017.1334310.

[22] Z. Wan, H. P. Wang, N. Chen, M. Wang and B. E. Carlson, Characterization of intermetallic compound at the interfaces of

Al-steel resistance spot welds, *J. Mater. Process. Technol*., 242 (2017) 12-23, doi: 10.1016/j.jmatprotec.2016.11.017.

[23] J. Kang, H. M. Rao, D. R. Sigler and B. E. Carlson, Tensile and fatigue behaviour of AA6022-T4 to if steel resistance spot welds, *Procedia Struct. Integr*., 5 (2017) 1425-1432, doi: 10.1016/j.prostr.2017.07.207.

[24] J. Chen, X. Yuan, Z. Hu, T. Li, K. Wu and C. Li, Improvement of resistance-spot-welded joints for DP 600 steel and A5052 aluminum alloy with Zn slice interlayer, *J. Manuf. Process*., 30 (2017) 396-405, doi: 10.1016/j.jmapro.2017.10.009.

[25] N. Chen, M. Wang, H. P. Wang, Z. Wan and B. E. Carlson, Microstructural and mechanical evolution of Al/steel interface with Fe2Al5 growth in resistance spot welding of aluminum to steel, *J. Manuf. Process*., 34 (2018) 424-434, doi: 10.1016/j.jmapro.2018.06.024.

[26] P. Podržaj, I. Polajnar, J. Diaci and Z. Kariž, Overview of resistance spot welding control, *Sci. Technol. Weld. Join*., 13 (3) (2008) 215-224, doi: 10.1179/174329308X283893.

[27] P. Prangnell, F. Haddadi and Y. C. Chen, Ultrasonic spot welding of aluminium to steel for automotive applications-microstructure and optimisation, *Mater. Sci. Technol*., 27 (3) (2011) 617-624, doi: 10.1179/026708310X520484.

[28] H. T. Fujii, Y. Goto, Y. S. Sato and H. Kokawa, Microstructure and lap shear strength of the weld interface in ultrasonic welding of Al alloy to stainless steel, *Scr. Mater*., 116 (2016) 135-138, doi: 10.1016/j.scriptamat.2016.02.004.

[29] F. Haddadi, D. Strong and P. B. Prangnell, Effect of zinc coatings on joint properties and interfacial reactions in aluminum to steel ultrasonic spot welding, *JOM*, 64 (3) (2012) 407-413, doi: 10.1007/s11837-012-0265-9.

[30] M. Shakil, N. H. Tariq, M. Ahmad, M. A. Choudhary, J. I. Akhter and S. S. Babu, Effect of ultrasonic welding parameters on microstructure and mechanical properties of dissimilar joints, *Mater. Des*., 55 (2014) 263-273, doi: 10.1016/j.matdes.2013.09.074.

[31] J. Mazumder, Laser heat treatment: the state of the art, *JOM*, 35 (5) (1983) 18-26, doi: 10.1007 /BF03338273.

[32] R. E. Wagner, Laser drilling mechanics, *J. Appl. Phys*., 45 (10) (1974) 4631-4637, doi: 10.1063/1.1663102.

[33] A. Mahrle and E. Beyer, Theoretical aspects of fibre laser cutting, *J. Phys. D. Appl. Phys*., 42 (17) (2009) doi: 10.1088/0022-3727/42/17/175507.

[34] D. Y. You, X. D. Gao and S. Katayama, Review of laser welding monitoring, *Sci. Technol. Weld. Join*., 19 (3) (2014) 181-201, doi: 10.1179/1362171813Y.0000000180.

[35] S. S. Lee, T. H. Kim, S. J. Hu, W. W. Cai and J. A. Abell, Joining technologies for automotive lithium-ion battery manufacturing - A review, *ASME 2010 Int. Manuf. Sci. Eng. Conf. MSEC 2010*, 1 (2010) 541-549, doi: 10.1115/MSEC2010-34168.

[36] L. H. Shah, F. Khodabakhshi and A. Gerlich, Effect of beam wobbling on laser welding of aluminum and magnesium alloy with nickel interlayer, *J. Manuf. Process*., 37 (2018) (2019) 212-219, doi: 10.1016/j.jmapro.2018.11.028.

[37] S. V. Kuryntsev and A. K. Gilmutdinov, The effect of laser beam wobbling mode in welding process for structural steels, *Int. J. Adv. Manuf. Technol*., 81 (9-12) (2015) 1683-1691, doi: 10.1007/s00170-015-7312-y.

[38] L. Wang, M. Gao, C. Zhang and X. Zeng, Effect of beam oscillating pattern on weld characterization of laser welding of AA6061-T6 aluminum alloy, *Mater. Des*., 108 (2016) 707-717, doi: 10.1016/j.matdes.2016.07.053.

[39] C. L. Druzgalski, A. Ashby, G. Guss, W. E. King, T. T. Roehling and M. J. Matthews, Process optimization of complex geometries using feed forward control for laser powder bed fusion additive manufacturing, *Addit. Manuf*., 34 (2020) 101169, doi: 10.1016/j.addma.2020.101169.

[40] L. Li and S. Anand, Hatch pattern based inherent strain prediction using neural networks for powder bed fusion additive manufacturing, *J. Manuf. Process*., 56 (2020) 1344-1352, doi: 10.1016/j.jmapro.2020.04.030.

[41] N. Nadammal et al., Effect of hatch length on the development of microstructure, texture and residual stresses in selective laser melted superalloy Inconel 718, *Mater. Des*., 134 (2017) 139-150, doi: 10.1016/j.matdes.2017.08.049.

[42] L. N. Trinh and D. Lee, The characteristics of laser welding of a thin aluminum tab and steel battery case for lithium-ion battery, *Metals*, 10 (6) (2020) 842, doi: 10.3390/met10060842.

[43] A. Mazzoli and O. Favoni, Particle size, size distribution and morphological evaluation of airborne dust particles of diverse woods by scanning electron microscopy and image processing program, *Powder Technol*., 225 (2012) 65-71, doi: 10.1016/j.powtec.2012.03.033.

[44] A. F. H. Kaplan and J. Powell, Spatter in laser welding, *J. Laser Appl*., 23 (3) (2011) 032005, doi: 10.2351/1.3597830.

[45] L. N. Trinh and D. Lee, Welding of thin tab and battery case for lithium-ion battery cylindrical cell using nanosecond pulsed fiber laser, *Journal of Welding and Joining*, 38 (4) (2020) 389-394, doi: 10.5781/jwj.2020.38.4.8.

[46] B. Bagheri, M. Abbasi, F. Sharifi and A. Abdollahzadeh, Investigation into novel multipass friction stir vibration brazing of carbon steels, *Mater. Manuf. Process*., 37 (8) (2022) 921-932, doi: 10.1080/10426914.2021.2006220.

[47] A. H. Vaneghi, B. Bagheri, A. Shamsipur, S. E. Mirsalehi and A. Abdollahzadeh, Investigations into the formation of intermetallic compounds during pinless friction stir spot welding of AA2024-Zn-pure copper dissimilar joints, *Weld. World*, 66 (11) (2022) 2351-2369, doi: 10.1007/S40194-022-01366-6/FIGURES/12.

[48] A. Abdollahzadeh, B. Bagheri, A. H. Vaneghi, A. Shamsipur and S. E. Mirsalehi, Advances in simulation and experimental study on intermetallic formation and thermomechanical evolution of Al-Cu composite with Zn interlayer: effect of spot pass and shoulder diameter during the pinless friction stir spot welding process, *Proceedings of the Institution of Mechanical Engineers, Part L: Journal of Materials: Design and Applications*, 237 (6) (2022) 1475-1494, doi: 10.1177/14644207221146981.

[49] X. Ao, H. Xia, J. Liu and Q. He, Simulations of microstructure coupling with moving molten pool by selective laser melting using a cellular automaton, *Mater. Des*., 185 (2020) 108230, doi: 10.1016/J.MATDES.2019.108230.

[50] J. Janesch, *Two-wire vs. Four-wire Resistance Measurements: Which Configuration Makes Sense for Your Application?*, Keithley, USA (2013) 2-4.

Dongkyoung Lee received his Ph.D. in Mechanical Engineering in 2012 and an M.S. in 2011, both from the University of Michigan, Ann Arbor, MI, U.S.A. He also earned an M.S. in Aerospace Engineering from the same university in 2017, and a B.S. in Mechanical Engineering from Hanyang University, Seoul, South Korea in 2006. Currently, he is an Associate (Tenured) Professor at Kongju National University, South Korea, in the Department of Mechanical and Automotive Engineering, Department of Future Convergence Engineering, and Center for Advanced Materials and Parts of Powder (CAMP^2). His research focuses on laser-aided manufacturing, with particular emphasis on applications in lithium-ion batteries, fuel cells, nuclear decommissioning, advanced semiconductor packaging, and display technologies.

Lanh Trinh obtained his M.S. in Engineering from Kongju National University, Cheonan, Korea, in 2021. During his master's program, his research specialized in laser welding for dissimilar metals in Lithium-ion batteries. Presently, he is pursuing a Ph.D. in Materials Engineering at the University of Nebraska-Lincoln, NE, U.S.A. His current research focuses on advanced manufacturing and fabrication of high entropy materials tailored for extreme environments, encompassing high temperature, corrosion, and irradiation.